Fatigue crack initiation prediction using phantom nodes-based extended finite element method for S355 and S690 steel grades

Xin, Haohui; Veljkovic, Milan

DOI
10.1016/j.engfracmech.2019.04.026

Publication date
2019

Document Version
Final published version

Published in
Engineering Fracture Mechanics

Engineering Fracture Mechanics 214 (2019) 164–176

Contents lists available at ScienceDirect

Engineering Fracture Mechanics

journal homepage: www.elsevier.com/locate/engfracmech

Fatigue crack initiation prediction using phantom nodes-based extended finite element method for S355 and S690 steel grades

Haohui Xin*, Milan Veljkovic

Faculty of Civil Engineering and Geosciences, Delft University of Technology, Netherlands

ARTICLE INFO

Keywords:
Fatigue crack initiation
Fatigue life prediction
Smith, Watson and Topper damage model
Phantom nodes
Extended finite element method (XFEM)

ABSTRACT

The assessment of fatigue crack initiation behavior of steel structures is essential and important especially to improve the application of high strength steel in construction. For a complete understanding of fatigue endurance, it is necessary to combine the phenomenological damage model with finite element numerical approach. In this paper, phantom nodes-based extended finite element method is used to predict the fatigue crack initiation of steel material, considering a prediction by XFEM of coupon tests made of steel grades S355 and S690. A user-defined fatigue damage initiation subroutine based on Smith, Watson, and Topper (SWT) damage model combined with non-linear isotropic/kinematic cyclic hardening model is implemented to predict fatigue crack initiation. The proposed method is successfully validated based on fatigue coupon test results of both steel grades, S355 and S690.

1. Introduction

The application of higher strength steel grades in construction is becoming attractive during the past two decades. High strength steels provide a potential for economical solutions for highly loaded slender members. Despite the benefits of the increased yield strength, the fatigue resistance of steel structures, both welded components and the base material, is one of the most important concerns [1].

Fatigue could be regarded as damage caused by the changes of microstructure leading to fatigue crack initiation followed by fatigue crack propagation under the time-dependent cyclic loading [2]. As is shown in Fig. 1, the fatigue process of a base steel material could be divided into two stages: (i) fatigue crack initiation period: micro-cracks initiated and gradually nucleated due to local accumulation dislocations, intra-granular fracture around inhomogeneous inclusions or other imperfections; (ii) fatigue crack propagation period: cracks under cyclic loading propagate through the mechanical element. Then, the fatigue life could be regarded as the sum of loading cycles in above two stages: (a) loading cycles which initiate a crack and (b) loading cycles which make the crack propagate to failure [3].

Fatigue crack initiation dominates the life of high-cycle fatigue and is a necessary step for fatigue crack propagation. The research on fatigue crack initiation is of highly practical significance both for the based material and for welded connections. Many studies have focused on addressing the physics of fatigue crack initiation in polycrystals based on the microstructure of material [3]. The importance of microstructure in determining fatigue damage accumulation and fatigue–microstructure relationship is highlighted by [6].

The fatigue crack initiation physics is based either on micro-grain scale analysis. However, the macro phenomenological damage

* Corresponding author.
E-mail address: H.Xin@tudelft.nl (H. Xin).

https://doi.org/10.1016/j.engfracmech.2019.04.026
Received 3 February 2019; Received in revised form 13 April 2019; Accepted 20 April 2019
Available online 24 April 2019
0013-7944/

Nomenclature

Latin characters

$\boldsymbol{a}_i$	the nodal enriched degree of freedom
b	material dependent parameter of Smith, Watson, and Topper (SWT) damage model
c	Material dependent parameter of Smith, Watson, and Topper (SWT) damage model
d_f	the damage index due to fatigue
E	Elastic modulus
f_{tol}	the tolerance of crack initiation criterion
f	the index of crack initiation criterion
G	the fracture energy release rate
G^C	the critical fracture energy release rate
K	strain hardening coefficient in the Ramberg-Osgood model
$H(x)$	the jump function
N	the total node number in the model
$N_i(x)$	the general shape functions
N_f	the number of loading cycles
n	the exponent in the Ramberg-Osgood model
$\boldsymbol{n}_{x^*}$	the unit outward normal to the crack at $\boldsymbol{x}^*$
r	Radius in the polar coordinate system with its origin at the crack tip
r_c	a specified nonlocal averaging radius;
$\mathbf{u}$	the displacement vector with the partition of unity enrichment
$\boldsymbol{u}_i$	the general nodal displacement vector associated to finite element solution
$\mathbf{x}$	is the position vector of a Gauss integration point
$\mathbf{x}^*$	is the position vector of a Gauss integration point

Greek characters

$\bar{\sigma}$	the nominal stress
σ	the true (Cauchy) stress
$\sigma_f^{'}$	material dependent parameter of Smith, Watson, and Topper (SWT) damage model
$\sigma_{n,\max}$	maximum normal stress on the principal strain range plane
$\bar{\varepsilon}$	the nominal strain
ε	the true (Cauchy) strain
$\varepsilon_f^{'}$	material dependent parameter of Smith, Watson, and Topper (SWT) damage model
$\Delta\varepsilon_1$	principal strain range

Subscripts

N_f	the damage index, stress or strain etc. at the cycle N_f
$N_f + x$	the damage index, stress or strain etc. at the cycle $N_f + x$
k	the loading cycle, cycle increment etc. at k^{th} step
$k + x$	The loading cycle, cycle increment etc. at $(k + x)^{\text{th}}$ step
n	the stress, strain etc. at the time counts n for each step
nn	the damage increment at sub fatigue cycle nn

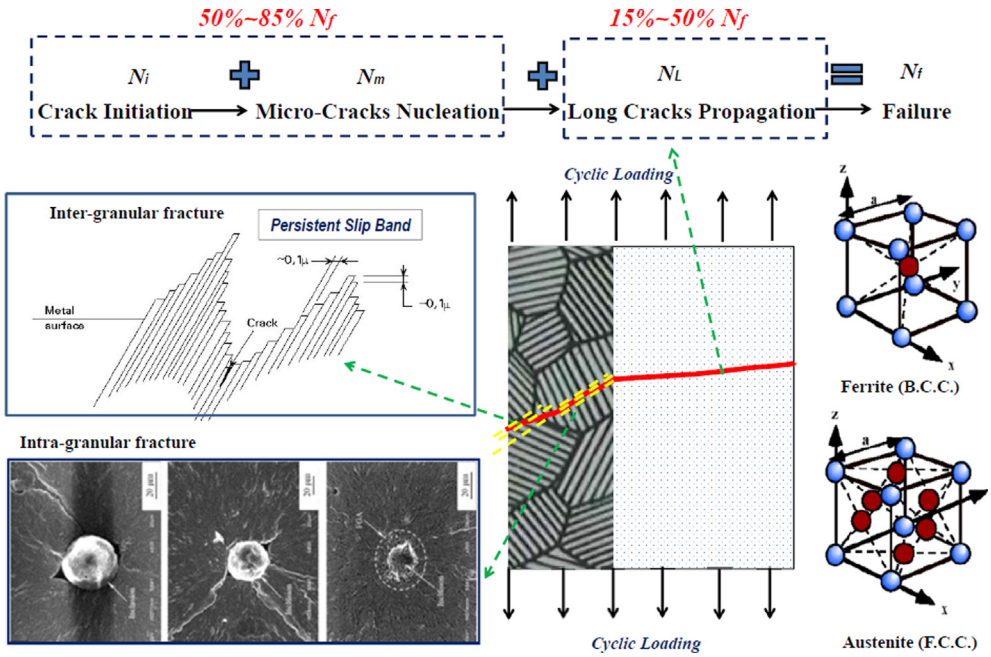

Fig. 1. Fatigue crack initiation and propagation of structural steels (Noted that this figure is organized based on references [4,5]).

method provides a methodology to derive models of fatigue life evolved from experimental observations of cracks nucleation and growth during cyclic loading. These models include stress-fatigue life method, strain-fatigue life method, stress/strain-fatigue life method, and energy-based fatigue life method [7,8,17,9–16] for uniaxial or multiaxial loading, in-phase (proportional) or out-of-phase (non-proportional) loading.

The stress-life method is the classical method for fatigue analysis of metals. *Wöhler* [18] recognized the stress range and the stress level as the main and secondary parameters governing the fatigue lifetime around 1850. After then, it became popular to plot fatigue life in terms of stress amplitude versus the number of cycles to failure, so-called *Wöhler* curve or *S–N* curve. Stresses in the steel structure are generally compared to the fatigue limit of the material. Basquin [19] firstly proposed a log-log relationship for S-N curves and is generally proposed in the design codes e.g. Eurocode 3 [20]. In addition, in order to account for the combined effect of the stress amplitude and the mean stress, the common models include Gerber model [21], Goodman Diagram [11], Soderberg equation [22], Morrow model [8] and Walker equation [9].

In terms of the strain-fatigue life method, the pioneer work is firstly proposed for low-cycle-fatigue of ductile metals under cyclic thermal loading, and is assumed that the plastic strain range controls the fatigue life by Coffin [23] and Manson [24], which has been further improved by Morrow [8] to obtain the total strain-fatigue life relationship and is known as Coffin-Manson-Morrow relationship.

For stress/strain-fatigue life method, Smith, Watson, and Topper [25] proposed that the product of the principal strain range and maximum stress in the principal strain range plane, known as SWT parameter, controls the fatigue life to consider the mean stress effects. SWT damage model could be used for both proportional and non-proportional loading situations. Fatemi and Socie [26] proposed FS parameter, which is the combination of the maximum shear strain amplitude and the maximum normal stress acting on the critical plane, to consider the crack closure effects. Based on the above SWT or FS critical plane approaches, fatigue life is usually dominated by microcrack growth either along the shear planes or along the tensile planes. Liu [27] proposed a virtual strain energy model (VSE) to consider both tensile failure and shear failure. While Liu's parameter was not originally formulated to include mean stress. One of the major effects of mean stress on microcracks is to alter the amount of crack closure. A mean stress correction on VSE model is added later [27].

The assessment of fatigue crack initiation behavior of steel structures is essential to predict fatigue behavior of structural components and it is necessary to combine the phenomenological damage model with finite element approach. Conventional finite element method (FEM) required mesh refinement to capture the singular asymptotic fields in the neighborhood of the crack tip, the mesh must be updated continuously to match the discontinuity as the crack growth progresses. The extended finite element approach (XFEM), firstly proposed by Belytschko in 1999 [28], alleviates above shortcomings by enriching the displacement vector. Later, the discontinuity was described by superposed elements and phantom nodes, and cracks are treated by adding phantom nodes and superposing elements on the original mesh [29]. Hence, phantom nodes-based extended finite element method is used to predict the fatigue crack initiation of steel structures as a pilot study in this paper. A user-defined fatigue damage initiation subroutine based on Smith, Watson, and Topper (SWT) damage model combined with non-linear isotropic/kinematic cyclic hardening model is implemented to predict fatigue crack initiation.

This paper is structured as follows: Section 2 details the material constitutive law of structural steels for the S355 and S690 steel grades; Section 3 explains the implementation of fatigue damage model in the user subroutine; Section 4 includes numerical examples of fatigue crack initiation; the last section presents some concluding remark and future research.

2. Material constitutive law

2.1. Uniaxial stress-strain relationship

Monotonic uniaxial stress-strain curves for the S355 and S690 steel grades are shown in Fig. 2 based on reference Jesus et al [30].

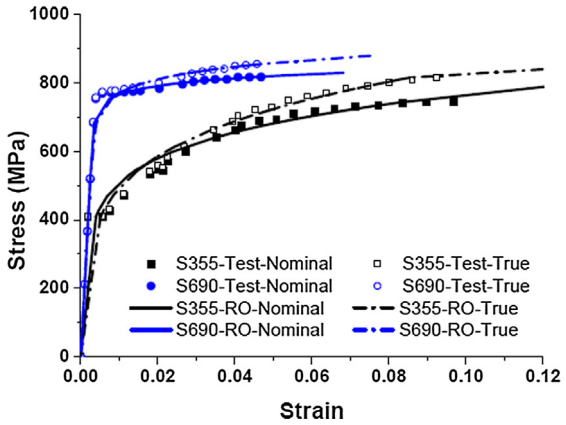

Fig. 2. Typical stress-strain relationship of the S355 and S690 steel grades [30].

True stress σ and true strain ε are calculated for an accurate definition of plastic behavior of ductile materials by considering the actual dimensions based on Eqs. (1) and (2).

$$\varepsilon=\ln(1+\bar{\varepsilon}) \tag{1}$$

$$\sigma=\bar{\sigma}(1+\bar{\varepsilon}) \tag{2}$$

The uniaxial stress-strain relationships for the S355 and S690 steel grades could be expressed by Ramberg-Osgood equation [31] listed in Eq.(3). The fitted parameters for the S355 and S690 steel grades were listed in Table 1. The comparisons between experimental results and the prediction of the Ramberg-Osgood model are shown in Fig. 2. A good agreement was observed.

$$\frac{\varepsilon}{2}=\frac{\sigma}{2E}+K\left(\frac{\sigma}{2E}\right)^{1/n} \tag{3}$$

2.2. Cyclic plasticity model

Multiaxial cyclic plasticity models are very important for the prediction of multiaxial fatigue crack initiation. The non-linear isotropic/kinematic cyclic hardening model presented in the ABAQUS software [32] is used to consider the plasticity for S355 and S690 steel grades. The kinematic hardening model with one back stress term is specified by a half-cycle input material data based on Ramberg-Osgood equation and Table 1. A comparison of stabilized stress-strain hysteresis loops between tests and non-linear isotropic/kinematic cyclic hardening model are shown in Figs. 3 and 4. The predicted results were generally comparable with experimental results. The FE simulation results tend to be a safe prediction because they are mostly larger than the experimental results. The possible reasons include: (i) the yield strength of structural steel at the high-stress level is much more dependent to hydrostatic pressure; (ii) the yield surface of the S355 and S690 steel grades may be rate dependent.

3. Implementation of fatigue crack initiation model

Modeling discontinuities as an enriched feature is an effective way to simulate the initiation and propagation of the discrete crack along an arbitrary, solution-dependent path without the requirement of re-meshing in the bulk materials [28]. Based on the concept of partition of unity, XFEM treated the cracks as a special enriched function in conjunction with additional degrees of freedom. The nodes are enriched with the jump function when the elements are intersected by a crack.

$$\mathrm{u}=\sum_{i=1}^{N} N_i(x)[\boldsymbol{u}_i + H(x)\boldsymbol{a}_i] \tag{4}$$

The jump function $H(x)$ for a crack is given by:

$$H(x)=\begin{cases} 1, & if\ (\boldsymbol{x}-\boldsymbol{x}^*)\cdot\boldsymbol{n}_{\boldsymbol{x}^*}\geq 0 \\ -1, & otherwise \end{cases} \tag{5}$$

As illustrated in Fig. 5, phantom nodes are superposed on the original real nodes aiming to represent the discontinuity of the cracked elements. When the fatigue crack initiation criterion is not reached, the element is intact and each phantom node is completely constrained to its corresponding real node. When the fatigue crack initiation criterion is fulfilled, the element is "cracked" and the element splits into two parts. Each part is formed by a combination of real and phantom nodes depending on the orientation of the crack. The separation between the phantom and the real nodes is governed by the cohesive law. The level set method is employed to describe the crack geometry by defining two orthogonal signed distance functions. One is used to describe the crack surface and the other is to build the orthogonal surface. Then, the intersection of those two surfaces gives the crack front.

In order to predict the fatigue crack initiation, the crack initiation criterion is expanded via a user-defined fatigue damage initiation subroutine (UDMGINI) based on Smith, Watson, and Topper (SWT) damage model [25] and implemented in ABAQUS software package [32]. The fatigue crack initiation damage index is defined as Eq. (6).

Table 1
Parameters of Ramberg-Osgood approximation.

Nominal stress	S355	K	626.90
		n	0.1618
	S690	K	466.08
		n	0.0338
True stress	S355	K	805.36
		n	0.2126
	S690	K	528.45
		n	0.0549

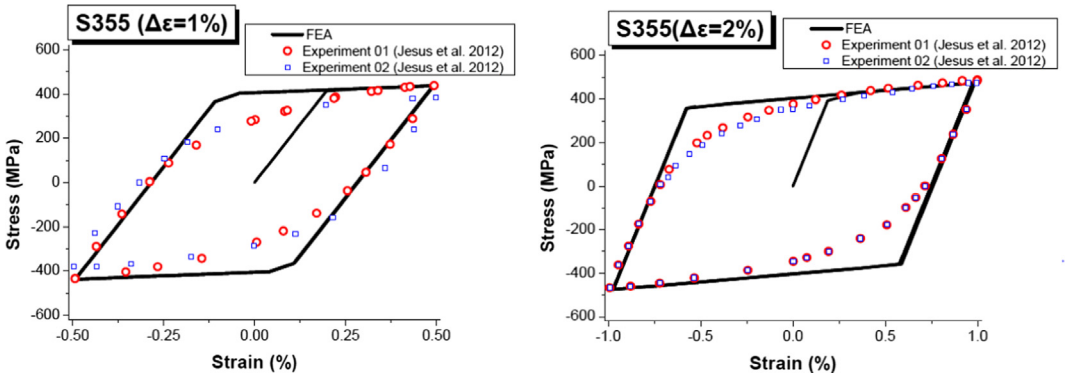

(a) Δε=1% (b) Δε=2%

Fig. 3. Stabilized stress-strain hysteresis loops comparisons of S355 steel grade.

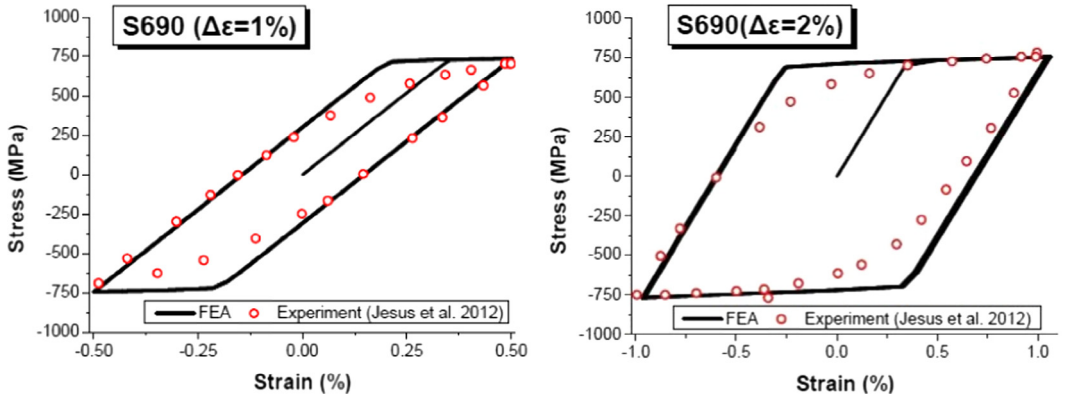

(a) Δε=1% (b) Δε=2%

Fig. 4. Stabilized stress-strain hysteresis loops comparisons of S690 steel grade.

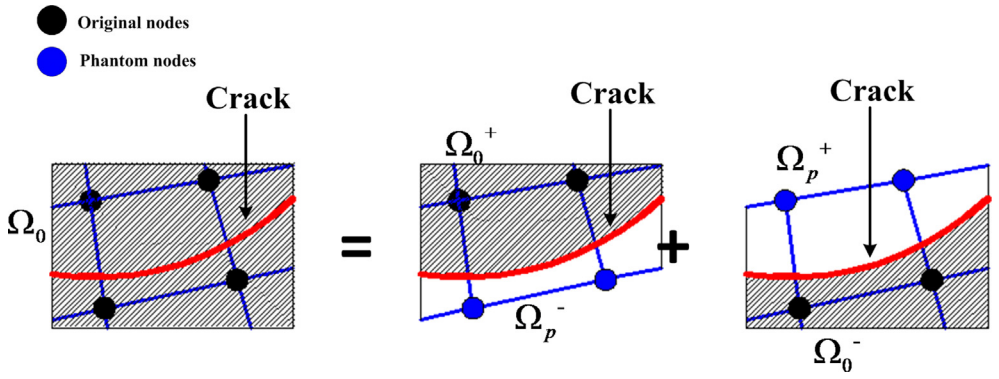

Fig. 5. The schematic of the phantom node method.

$$d_f = \frac{\frac{1}{2}\sigma_{n,\max}\Delta\varepsilon_1}{\frac{\sigma_f^{'2}}{E}(2N_f)^{2b} + \sigma_f^{'}\varepsilon_f^{'}(2N_f)^{b+c}} \tag{6}$$

Taking the derivation of the fatigue crack initiation criterion to the number of loading cycles, yields:

$$\frac{\partial d_f}{\partial N_f} = \frac{\frac{1}{2}\sigma_{n,\max}\Delta\varepsilon_1\left[\frac{2b\sigma_f^{'2}}{E}(2N_f)^{2b-1} + (b+c)\sigma_f^{'}\varepsilon_f^{'}(2N_f)^{b+c-1}\right]}{\left[\frac{\sigma_f^{'2}}{E}(2N_f)^{2b} + \sigma_f^{'}\varepsilon_f^{'}(2N_f)^{b+c}\right]^2} \tag{7}$$

The fatigue crack initiation index is updated based on the forward Euler method [33] as Eq. (8). When the fatigue crack initiation damage index increased larger than 1.0, the crack initiation criterion f will be defined as 1.025.

$${}^{N_f+\Delta N}d_f = {}^{N_f}d_f + \frac{\partial d_f}{\partial N_f}\Delta N \tag{8}$$

A crack is established or the crack length of an existing crack is extended when the fatigue cracks initiation criterion f, see Eq. (15), reached the value 1.0, within a given tolerance as Eq. (9). The newly introduced crack is assumed orthogonal to the maximum principal strain direction when the fatigue crack initiation criterion is satisfied.

$$1.0 \le f \le 1.0 + f_{tol} \tag{9}$$

The tolerance of crack initiation criterion f_{tol} is assumed to be 0.05. It is also the reason the parameter f is defined as 1.025 when

Box 1
Implementation algorithm of fatigue crack initiation damage model.

1. **Update the fatigue loading cycles with specified cycle increment** ${}^{k+1}\Delta N_f$
   ${}^{k+1}N_f = {}^{k}N_f + {}^{k+1}\Delta N_f$
   1–1: IF ${}^{k+1}N_f \leqslant {}^{max}N_f$, THEN GO TO 2;
   1–2: IF ${}^{k+1}N_f > {}^{max}N_f$, THEN STOP;
2. **Update the maximum normal stress and principal strain range:**
   2–1: Initial solution-dependent variables:
   n = 0; $tt = 0$; $\sigma_{n,max} = 0$; $\varepsilon_{1,max=0}$; $\varepsilon_{3,min=0}$; $\Delta\varepsilon_1 = 0$
   2–2: IF $tt > T$; THEN GO TO 2–4; (T *is period for periodic amplitude*)
   2–3: IF $tt \le T$; THEN:
   2–3-1: Initial variables:
   ${}^{n}\sigma_{n,max} = \sigma_{n,max}$;
   ${}^{n}\varepsilon_{1,max} = \varepsilon_{1,max}$;
   ${}^{n}\varepsilon_{3,min} = \varepsilon_{3,min}$;
   2–3-2: Update $\sigma_{n,max}$:
   $\sigma_{n,max} = MAX({}^{n+1}\sigma_{n,max,}\ {}^{n}\sigma_{n,max})$
   2–3-3: Update $\varepsilon_{1,max}$: IF $tt < \frac{T}{2}$, TEHN:
   $\varepsilon_{1,max=MAX(}\ {}^{n+1}\varepsilon_{1,max},\ {}^{n}\varepsilon_{1,max})$
   2–3-4: Update $\varepsilon_{3,min}$: IF $tt > \frac{T}{2}$, TEHN:
   $\varepsilon_{3,min=MIN(}\ {}^{n+1}\varepsilon_{3,min},\ {}^{n}\varepsilon_{3,min})$
   2–3-5: GO TO 2–2 for next time increment, $tt = tt + \Delta t$; $n = n + 1$.
   2–4: Calculate principal strain range: $\Delta\varepsilon_1 = \varepsilon_{1,max} - \varepsilon_{3,min}$; THEN GO TO 3;
3. **Update the fatigue crack initiation index:**
   3–1: Initial solution-dependent variables:
   $nn = 1$;
   3–2: IF $nn > {}^{k+1}\Delta N_f$; THEN GO TO 3–6;
   3–3: IF $nn \leqslant {}^{k+1}\Delta N_f$; THEN:

$$nn\frac{\partial d_f}{\partial N_f} = \frac{\frac{1}{2}\sigma_{n,\max}\Delta\varepsilon_1\left[\frac{2b\sigma_f^{'2}}{E}[2({}^{k}N_f+nn)]^{2b-1} + (b+c)\sigma_f^{'}\varepsilon_f^{'}[2({}^{k}N_f+nn)]^{b+c-1}\right]}{\left[\frac{\sigma_f^{'2}}{E}[2({}^{k}N_f+nn)]^{2b} + \sigma_f^{'}\varepsilon_f^{'}[2({}^{k}N_f+nn)]^{b+c}\right]^2}$$

   3–4: Update the fatigue crack index,

$${}^{N_f+nn}d_f = {}^{N_f+nn-1}d_f + MAX\left(nn\frac{\partial d_f}{\partial N_f}, 0\right)$$

   3–5: GO TO 3–2 for next loading cycle, nn = nn + 1;
   3–6: IF ${}^{N_f+\Delta N}d_f \geqslant 1.0$; THEN: $f = 1.025$; ELSE: $f = 0$;
   3–7: GO TO 1;

fatigue crack initiated. Sensitivity simulations showed that the difference is tiny when fatigue cracks initiation criterion *f is* defined as a value between 1.0 and 1.05.

After the fatigue crack initiation criterion is achieved, the damage evolution law similar to surface based cohesive behavior is used to predict fatigue crack propagation. The power law (Eq. (10)) is employed to consider a mixed mode crack propagation.

$$\frac{G_{eq}}{G_{eq}^{c}} = \left(\frac{G_I}{G_I^{c}}\right)^{n} + \left(\frac{G_{II}}{G_{II}^{c}}\right)^{n} + \left(\frac{G_{III}}{G_{IIII}^{c}}\right)^{n} \tag{10}$$

The detailed implementation algorithm is summarized in Box 1. The flow chart of the implementation algorithm of fatigue crack initiation damage model is shown in Fig. 6.

It is noted that, for isotropic plastic material, different asymptotic crack-tip functions are required in each iteration depending on the crack location and the extent of the inelastic material deformation, accurately modeling the crack-tip singularity requires constantly keeping track of where the crack propagates and is relatively cumbersome because the degree of crack singularity depends on the location of the crack. The moving cracks are modeled by the cohesive segments method and phantom nodes based on traction separation cohesive behavior. The displacement jump across a cracked element is considered and the crack propagates across an entire element at a time to avoid the need to model the stress singularity. Thus, the stress field around the crack tip is not accurate due

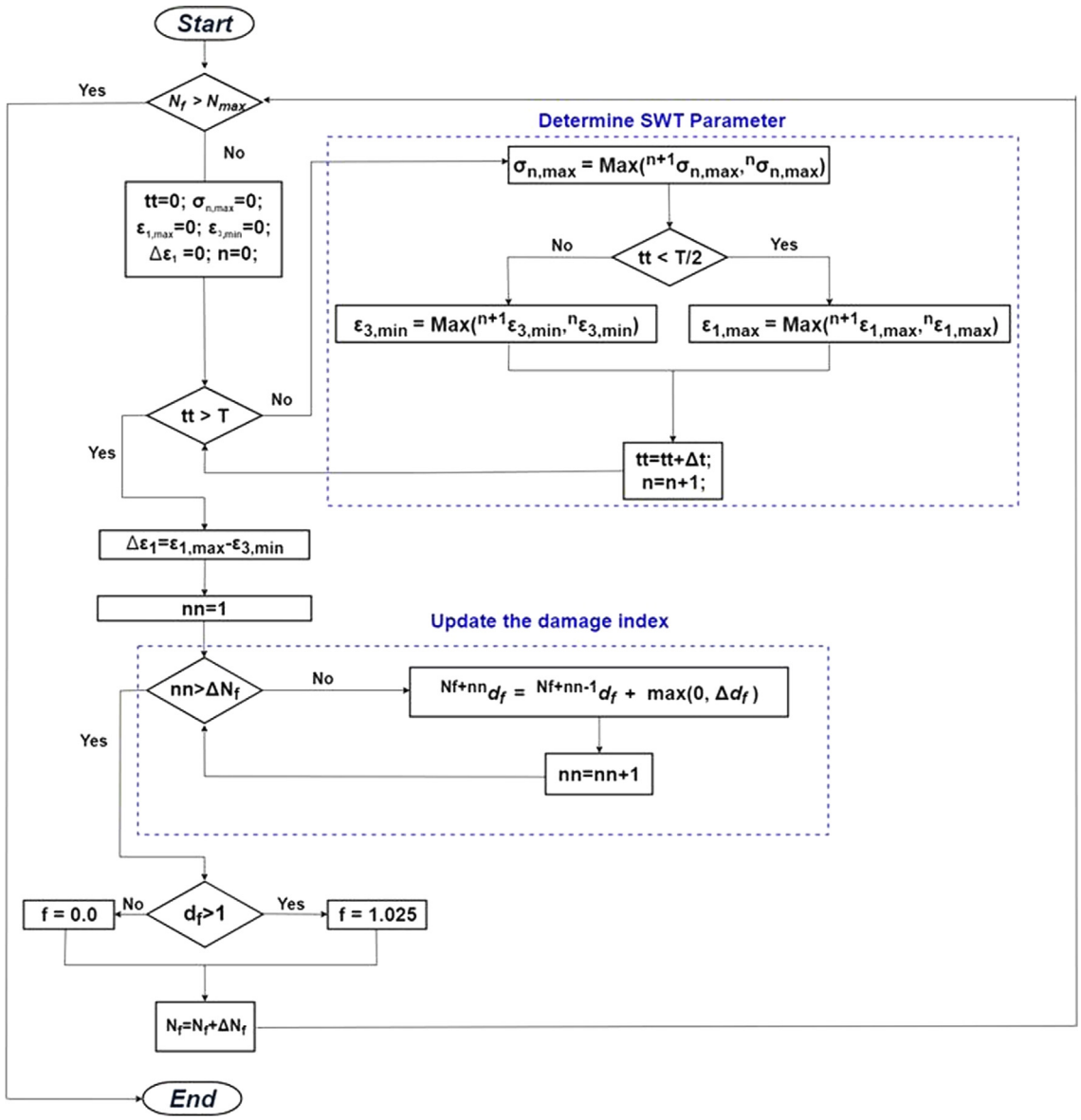

Fig. 6. Implementation flow chart of fatigue crack initiation damage model.

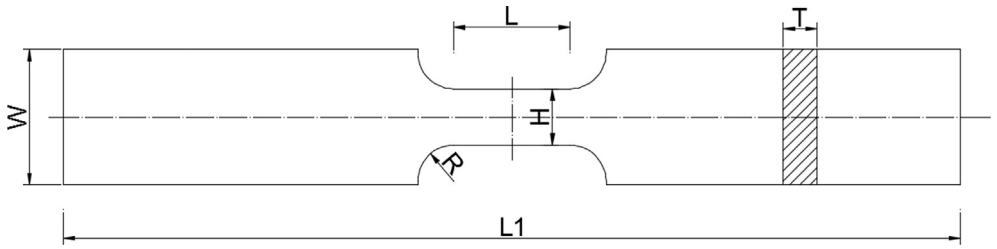

Fig. 7. Geometry of specimens used in the fatigue tests [30].

Table 2
Nominal dimensions of the specimens [30].

Material	W (mm)	T (mm)	L (mm)	L_1 (mm)	H (mm)	R (mm)
S355	30	7.5	26	200	12.5	8
S690	16	4	13	110	8	4.5

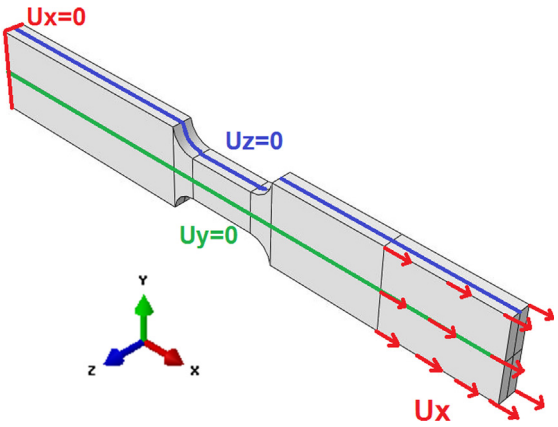

Fig. 8. Finite element model of the specimens used in the fatigue tests.

Table 3
Parameters of SWT damage model for S355 and S690 Steel Grades [30].

Materials	σ_f'	ε_f'	b	c
S355	952.2	0.7371	−0.089	−0.664
S690	1403.0	0.7396	−0.087	−0.809

to neglect the stress singularity. A Gaussian function is used as a weighting scheme for average stress/strain ahead of the crack tip to improve the crack propagation direction as shown in Eq. (11). The r_c is assumed as three times the typical characteristic length in the enriched region.

$$\omega(r) = \frac{1}{(2\pi)^{3/2} r_c^3} e^{\left(-\frac{r^2}{2r_c^2}\right)} \tag{11}$$

4. Numerical examples

In this section, the proposed fatigue crack initiation method is validated comparing the results obtained from the numerical simulation with the results provided by the experiment presented in Jesus et al. [30]. The geometry of the specimens for the S355 and S690 steel grades is shown in Fig. 7 and Table 2 based on the reference [30] in accordance with the recommendation of ASTM E606 [34]. The finite element model and boundary conditions are shown in Fig. 8. C3D8 element [32] is used during the simulations. The Z-translation in the middle line of the top and bottom surface of specimens is fixed and the Y-translation in the middle line of the front and back surface is fixed. The X-translation of one end surface is fixed, and the strain amplitude in fatigue load is achieved by the axial periodic displacement Ux at the side surface of the other end. The non-linear isotropic/kinematic cyclic hardening model

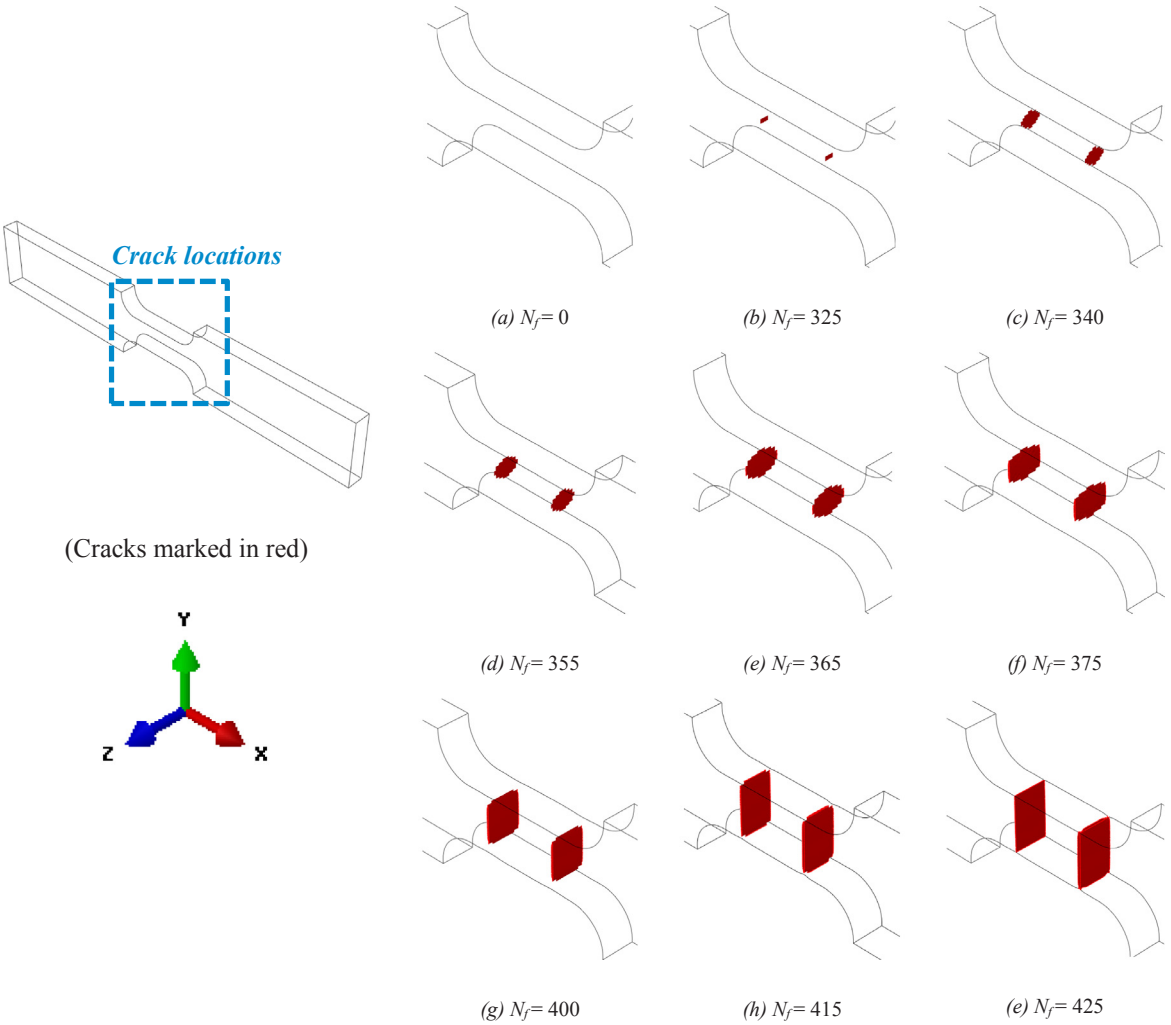

Fig. 9. Fatigue crack initiation and propagation for S355 with strain amplitude of 2%.

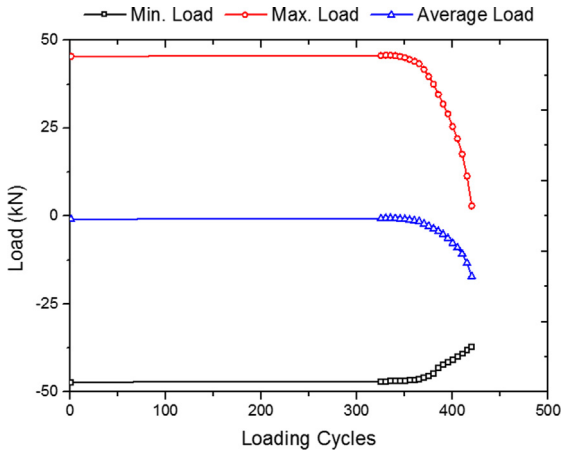

Fig. 10. Different Load level .vs. fatigue loading cycles.

detailed in Section 2 is used to describe the multiaxial cyclic plasticity for the S355 and S690 steel grade. The parameters of the SWT damage model for the S355 and S690 steel grades were summarized in Table 3 based on the reference [30]. The critical fracture energy release rate is assumed as a small value (0.01 N/mm) to make sure that the SWT damage model-based fatigue cracks initiation

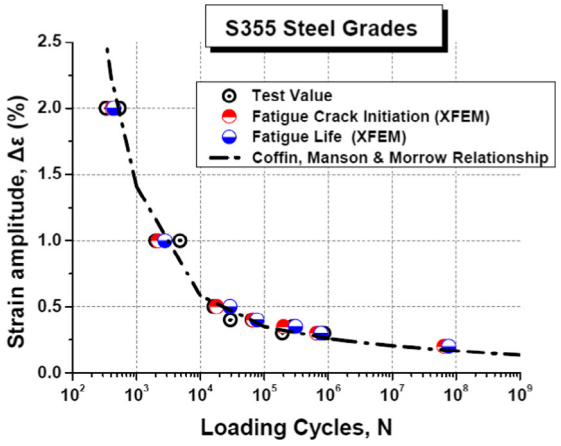

(a) S355

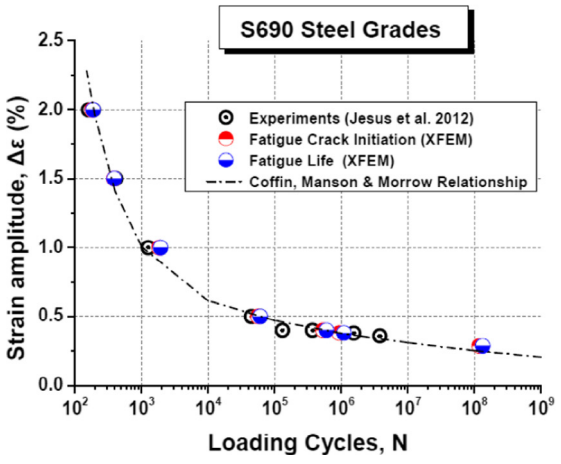

(b) S690

Fig. 11. Fatigue life comparisons between experiments and XFEM prediction.

Table 4
Fatigue life comparisons between experiments [30] and the XFEM predictions.

Steel	Strain Amplitude	Experiments			XFEM		XFEM /Average	
		Test 1	Test 2	Average	Initiation	Failure	Initiation	Failure
S355	2%	336	542	439	325	425	74.0%	96.8%
	1%	4805	2009	3407	2080	2790	61.1%	81.9%
	0.5%	16,175	–	16,175	17,300	19,400	107.0%	119.9%
	0.4%	–	64,244	64,244	61,800	72,800	96.2%	113.3%
	0.35%	278,243	–	278,243	200,200	306,000	72.0%	110.0%
	0.3%	–	861,304	861,304	587,800	738,600	68.2%	85.8%
S690	2.0%	190	160	175	150	188	85.7%	107.4%
	1.5%	410	–	410	370	415	90.2%	101.2%
	1.0%	1272	1920	1596	1780	1900	111.5%	119.0%
	0.5%	60,505	44,819	52,662	52,000	58,600	98.7%	111.3%
	0.4%	–	371,000	371,000	456,000	480,000	122.9%	129.4%
	0.36%	1,545,579	–	1,545,579	1,250,000	1,420,000	80.9%	91.9%

method will dominate during the simulations. The value of critical energy release rate for mode II and III is assumed to be the same as mode I for lack of experimental data. It is noted that the critical energy release rate for mode I is dominated in this study, the value for mode II and III needed to be further calibrated or tested for shear-dominated failure mode. The exponent of power-law used for crack propagation is assumed to be 2.0. It is noted that the fracture energy release rate should be smaller enough for the fatigue initiated

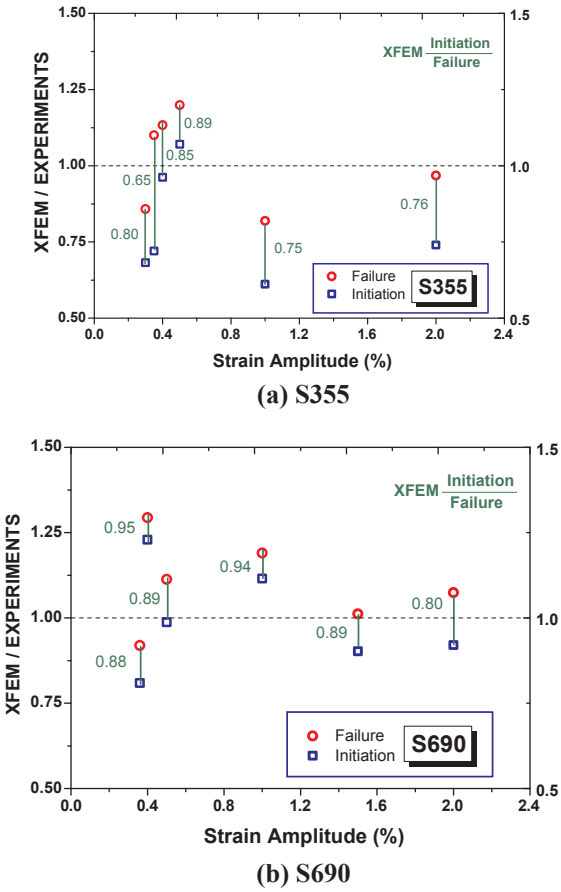

Fig. 12. Fatigue behavior comparisons between mild steel S355 and high strength steel S690.

cracks, and the fracture energy release rate should be same as the ductile fracture for the static cracks propagation in each loading cycles. Different critical fracture energy release rate will be assumed for the fatigue initiated cracks and static crack propagation during each cycle in the near future. In order to improve the convergence, automatic stabilization is defined with specified dissipated energy fraction of 0.002. The adaptive stabilization with a maximum ratio of stabilization to strain energy is defined as 0.05.

A typical fatigue crack initiation and propagation for S355 specimens with the strain amplitude 2% is shown in Fig. 9. The numerical simulation results showed that fatigue cracks initiated in the narrower part of the specimen at the loading cycle of 325, as shown in Fig. 9b. Due to the limitation that the crack only propagates across an entire element at a time, the shape of the initial fatigue crack presented as a small rectangular. Two fatigue cracks initiated at the same time due to symmetric mesh and boundary. It is noted that fatigue cracks generally occurred at one certain position in the real situation due to the material (and/or) geometry imperfections and possible an un-symmetric loading. When the loading cycles increased from 325 to 355, the shape of cracks gradually tended to be circular. As is shown in Fig. 9e, the fatigue cracks propagated through the thickness direction when the loading cycles reached 365. After then, the fatigue cracks propagated along the width (the y-direction). Hence, the shapes of fatigue cracks gradually changed to a rectangular when the load cycles increased from 375 to 415. The specimens failed at the loading cycle 425 when one fatigue crack propagated through the whole cross-section.

The relationship between different load level and fatigue load cycles is shown in Fig. 10 for S355 steel grades under strain-controlled loading strategies. The results showed that the maximum load gradually decreased, but the minimum load gradually increased when the fatigue crack initiated. The average load tended to be in compressive when the crack gradually propagated. It is because the general contact is considered in the cracked cross-section, the tensile load decreased faster than the compressive load.

The fatigue life comparisons between experimental results and XFEM predictions were shown in Fig. 11. A successful prediction of the fatigue behavior of coupon specimens made of S355 mild steel and S690 high strength steel is achieved. The detailed fatigue life of experimental results and XFEM predictions are listed in Table 4. Scattering of 8 coupon experiments, S355 steel, is in a range of ± 20% for the number of cycles for the fatigue resistance. Scattering of 9 coupon experiments, S690 steel, is in a range of ± 30% for the number of cycles for the fatigue endurance. It is noted that the relatively large difference is mainly due to the large scatter of experimental results. Probabilistic SWT damage model is expected to combine with phantom nodes-based extended finite element method in the near future.

The fatigue behavior comparison between mild steel S355 and high strength steel S690 is shown in Fig. 12. The results show that

the ratio between XFEM-based fatigue crack initiation loading cycles and fatigue failure loading cycles $R_{initiation/failure}$ is relatively higher for the smaller strain amplitude. The $R_{initiation/failure}$ of S355 steels compare to S690 is relatively smaller at the smaller strain amplitude. For the larger strain amplitude, the ratio $R_{initiation/failure}$ is relatively smaller compare with $R_{initiation/failure}$ at the smaller strain amplitude due to larger effects from plastic strain. In addition, the ratio $R_{initiation/failure}$ of S355 is smaller than in case of S690, which means that the S690 coupons specimens show more brittle behavior compared with S355.

5. Conclusions and future research

Below conclusions could be obtained based on the above discussions:

(1) Phantom nodes-based extended finite element method is used to predict the fatigue crack initiation of steel structures. A user-defined fatigue damage initiation subroutine based on Smith, Watson, and Topper (SWT) damage model combined with non-linear isotropic/kinematic cyclic hardening model is implemented to predict fatigue crack initiation.
(2) The proposed method is successfully validated using coupon tests of S355 and S690 steel grades. Scattering of 8 coupon experiments, S355 steel, is in a range of +/- 20% for the number of cycles for the fatigue resistance. Scattering of 9 coupon experiments, S690 steel, is in a range of +/- 30% for the number of cycles for the fatigue endurance. It is noted that the relatively large difference is mainly due to the large scatter of experimental results.
(3) The ratio between XFEM-based fatigue crack initiation loading cycles and fatigue failure loading cycles $R_{initiation/failure}$ is relatively higher for the smaller strain amplitude. The $R_{initiation/failure}$ of S355 steels compare to S690 is relatively smaller at the smaller strain amplitude. For the larger strain amplitude, the ratio $R_{initiation/failure}$ is relatively smaller compared with $R_{initiation/failure}$ at the smaller strain amplitude due to larger effects from the plastic strain. In addition, the ratio $R_{initiation/failure}$ of S355 is smaller than in the case of S690, which means that the S690 coupons specimens show more brittle behavior compared with S355.

Present fatigue crack initiation prediction method could be further extended in the following aspects:

(1) Critical plane approach methods could be used to calculate the parameter SWT to consider non-proportional loading; The stress singularity around the crack tip need to be further improved; the phantom nodes-based extended finite element method could be extended to other models, like FS parameter and energy-based damage model.
(2) The weighting schemes for nonlocal averaging could be improved to make fatigue crack initiation mesh independent;
(3) Probabilistic SWT damage model is expected to combine with phantom nodes-based extended finite element method.

References

[1] Macdonald K. Fracture and fatigue of welded joints and structures. Elsevier; 2011.
[2] Fajdiga G, Sraml M. Fatigue crack initiation and propagation under cyclic contact loading. Eng Fract Mech 2009;76:1320–35.
[3] Sangid MD. The physics of fatigue crack initiation. Int J Fatigue 2013;57:58–72.
[4] Lawrence FV, Jones RC. Mechanisms of fatigue crack initiation and growth. Met Trans 1970;1:367–93.
[5] Tanaka K, Mura T. A theory of fatigue crack initiation at inclusions. Metall Trans A 1982;13:117–23.
[6] Shyam A, Jha SK, Caton MJ. Preface to special issue on fatigue and microstructure. Int J Fatigue 2013;1.
[7] Correia JAFdeO, Blasón S, De Jesus AMP, Canteli AF, Moreira P, Tavares PJ. Fatigue life prediction based on an equivalent initial flaw size approach and a new normalized fatigue crack growth model. Eng Fail Anal 2016;69:15–28.
[8] Morrow J. Cyclic plastic strain energy and fatigue of metals. Intern. Frict. damping. Cycl. Plast., ASTM International 1965.
[9] Walker K. The effect of stress ratio during crack propagation and fatigue for 2024–T3 and 7075–T6 aluminum. Eff. Environ. complex load Hist. fatigue life. ASTM International; 1970.
[10] Liao D, Zhu S-P, Correia JAFO, De Jesus AMP, Calçada R. Computational framework for multiaxial fatigue life prediction of compressor discs considering notch effects. Eng Fract Mech 2018;202:423–35.
[11] Goodman J. Mechanics applied to engineering. Green: Longmans; 1918.
[12] Zhu S-P, Liu Q, Peng W, Zhang X-C. Computational-experimental approaches for fatigue reliability assessment of turbine bladed disks. Int J Mech Sci 2018;142:502–17.
[13] Abaqus V. 6.14 Documentation. Dassault Syst Simulia Corp; 2014;651.
[14] Park JU, An G, Woo W. The effect of initial stress induced during the steel manufacturing process on the welding residual stress in multi-pass butt welding. Int J Nav Archit Ocean Eng 2018;10:129–40. https://doi.org/10.1016/j.ijnaoe.2017.02.007.
[15] Qian G, Lei WS, Peng L, Yu Z, Niffenegger M. Statistical assessment of notch toughness against cleavage fracture of ferritic steels. Fatigue Fract Eng Mater Struct 2018;41:1120–31. https://doi.org/10.1111/ffe.12756.
[16] Zhu SP, Lei Q, Huang HZ, Yang YJ, Peng W. Mean stress effect correction in strain energy-based fatigue life prediction of metals. Int J Damage Mech 2017;26:1219–41. https://doi.org/10.1177/1056789516651920.
[17] Qian G, Cao Y, Niffenegger M, Chao YJ, Wu W. Comparison of constraint analyses with global and local approaches under uniaxial and biaxial loadings. Eur J Mech A/Solids 2018;69:135–46. https://doi.org/10.1016/j.euromechsol.2017.12.006.
[18] Wöhler A. Über die Festigkeits-versuche mit Eisen und. Stahl. 1870.
[19] Basquin OH. The exponential law of endurance tests. Proc Am Soc Test Mater 1910;10:625–30.
[20] European Committee for Standardization (CEN). EN 1993-1-9: Eurocode 3:Design of steel structures, part 1–9: fatigue. Brussels: European standard; 2004.
[21] Gerber WZ. Investigation of the allowable stress in iron construction. Bayer Arch Ing Ver (Bavarian Arch Eng Assoc) 1874;6:101.
[22] Soderberg CR. Factor of safety and working stress. Trans Am Soc Mech Eng 1939;52:13–28.
[23] Coffin Jr LF. A study of the effects of cyclic thermal stresses on a ductile metal. Trans Am Soc Mech Eng New York 1954;76:931–50.
[24] Manson SS. Behavior of materials under conditions of thermal stress; 1954.
[25] Smith KN, Toper T, Watson P. A stress-strain function for the fatigue of metals. J Mater 1970;5:767–78.
[26] Fatemi A, Socie DF. A critical plane approach to multiaxial fatigue damage including out-of-phase loading. Fatigue Fract Eng Mater Struct 1988;11:149–65.
[27] Liu KC. A method based on virtual strain-energy parameters for multiaxial fatigue life prediction. Adv. multiaxial fatigue. ASTM International; 1993.
[28] Moës N, Dolbow J, Belytschko T. A finite element method for crack growth without remeshing. Int J Numer Methods Eng 1999;46:131–50.

[29] Song J, Areias PMA, Belytschko T. A method for dynamic crack and shear band propagation with phantom nodes. Int J Numer Methods Eng 2006;67:868–93.
[30] De Jesus AMP, Matos R, Fontoura BFC, Rebelo C, Simões Da Silva L, Veljkovic M. A comparison of the fatigue behavior between S355 and S690 steel grades. J Constr Steel Res 2012;79:140–50. https://doi.org/10.1016/j.jcsr.2012.07.021.
[31] Ramberg W, Osgood WR. Description of stress-strain curves by three parameters; 1943.
[32] Abaqus V. 6.14 Documentation. Dassault Syst Simulia Corp; 2014.
[33] Belytschko T, Liu WK, Moran B, Elkhodary K. Nonlinear finite elements for continua and structures. John wiley & sons; 2013.
[34] Standard, ASTM. E606-92,“Standard Practice for Strain-Controlled Fatigue Testing,” Annual Book of ASTM Standards; 2004.